Accepted in ApJ Letters

On the nature of the tertiary companion to FW Tau: ALMA CO observations and SED modeling

Claudio Caceres[1,10], Adam Hardy[1,10], Matthias R. Schreiber[1,10], Héctor Cánovas[1,10], Lucas A. Cieza[2,10], Jonathan P. Williams[3], Antonio Hales[4,5], Christophe Pinte[6,7], Francois Ménard[7,8], Zahed Wahhaj[9]

ABSTRACT

It is thought that planetary mass companions may form through gravitational disk instabilities or core accretion. Identifying such objects in the process of formation would provide the most direct test for the competing formation theories. One of the most promising candidates for a planetary mass object still in formation is the third object in the FW Tau system. We here present ALMA cycle 1 observations confirming the recently published 1.3 mm detection of a dust disk around this third object and present for the first time a clear detection of a single peak ^{12}CO (2–1) line, providing direct evidence for the simultaneous existence of a gas disk. We perform radiative transfer modeling of the third object

[1]Instituto de Física y Astronomía, Universidad de Valparaíso, Av. Gran Bretaña 1111, 2360102 Valparaíso, Chile

[2]Núcleo de Astronomía, Universidad Diego Portales, Av. Ejército 441, Santiago, Chile

[3]Institute for Astronomy, University of Hawaii at Manoa, Honolulu, HI 96822, USA

[4]Atacama Large Millimeter/Submillimeter Array, Joint ALMA Observatory, Alonso de Córdova 3107, Vitacura 763-0355, Santiago - Chile

[5]National Radio Astronomy Observatory, 520 Edgemont Road, Charlottesville, Virginia, 22903-2475, United States

[6]Univ. Grenoble Alpes, IPAG, F-38000 Grenoble, France CNRS, IPAG, F-38000 Grenoble, France

[7]UMI-FCA, CNRS/INSU, France (UMI 3386)

[8]Departamento de Astronomía, Universidad de Chile, Camino del Observatorio 1515, Las Condes, Santiago, Chile

[9]European Southern Observatory, Av. Alonso de Córdova 3107, Vitacura, 19001 Santiago, Chile

[10]ICM nucleus on protoplanetary disks, Universidad de Valparaíso, Av. Gran Bretaña 1111, 2360102 Valparaíso, Chile

in FW Tau and find that current observations are consistent with either a brown dwarf embedded in an edge-on disk or a planet embedded in a low inclination disk, which is externally irradiated by the binary companion. Further observations with ALMA, aiming for high SNR detections of non contaminated gas lines, are required to conclusively unveil the nature of the third object in FW Tau.

Subject headings: circumstellar matter — protoplanetary disks — stars: individual (FW Tau) — planetary systems — techniques: interferometric

1. Introduction

Planetary mass companions (PMC) at wide separations often exceeding 100 au have been relatively frequently found in recent direct imaging surveys (e.g. Neuhäuser et al. 2005; Lafrenière et al. 2008; Schmidt et al. 2008; Ireland et al. 2011; Bailey et al. 2014). If relatively close, i.e. at separations $\lesssim 100$ au, PMCs may form through the classical mechanisms of core accretion (Lissauer & Stevenson 2007) or Class II gravitational instabilities (Boss 1997, 2011). At larger separations, disk fragmentation at the Class 0/I stages seems to be more likely (Kratter et al. 2010). Due to their large separations from their host stars, these objects are probably the most promising candidates to directly observe and characterize circumplanetary disks that may have formed either from the surrounding cloud or from the massive disk around the host star. Indirect evidence for the presence of such disks around several PMCs has been provided recently by the detection of emission lines or possible mid-infrared excesses that might be related to disks and outflows (e.g. Seifahrt et al. 2007; Schmidt et al. 2008; Bowler et al. 2014), and large optical/ultraviolet excess emission, potentially indicating the presence of shocks produced during the accretion process (Zhou et al. 2014).

One of the most convincing candidates for a disk around a potential PMC has been recently provided by the third component in the triple system FW Tau. This system belongs to the nearby ($d \sim 140$ pc) and young (~ 2 Myr) Taurus-Auriga star forming region (Goldsmith et al. 2008). The primary in FW Tau consists of a close binary, composed of two M5 stars, with a projected separation of 11 au (75 mas). The faint tertiary component has been first reported by White & Ghez (2001) and confirmed to be co-moving at a projected separation of 330 au by Kraus et al. (2014). The primary binary in FW Tau is not showing evidence for the presence of accretion (Cieza et al. 2012) while for the third object indications for accretion have been found (Bowler et al. 2014).

Moreover, Kraus et al. (2015, hereafter K2015) have recently derived a dust disk mass of 1–2 $M_\oplus$, based on their ALMA band 6 continuum observations. While their observations also

cover the ^{12}CO (2–1) line, their observational setup used wide velocity channels (20 km s^{-1}) and the line remained undetected. Despite these constraints however, the nature of the tertiary companion in the FW Tau system has remained unclear, as the near-IR photometry and spectroscopy is consistent with both a planetary mass object with accretion-induced veiling, or a brown dwarf or low-mass star with spectral types M5–M8 embedded in an edge-on disk (Bowler et al. 2014).

Here we present a clear detection of the ^{12}CO (2–1) line towards the tertiary companion to FW Tau and construct the spectral energy distribution (SED) of the system from near-IR to the millimeter wavelengths. Using radiative transfer and CO-line disk modeling we explore the two proposed scenarios.

2. ALMA cycle 1 observations: continuum and gas detection

We observed FW Tau with ALMA in Cycle 1 on 2013 December 4. We obtained one epoch observation in band 6, with the correlator configured to obtain one baseband centered at 230.52 GHz which was aimed at detecting the ^{12}CO (2–1) spectral line, and three continuum basebands centered at 228.52, 214.52, and 212.52 GHz. The total bandwidth for the observations was 7.5 GHz, with a unique spectral spacing of 488.28 kHz in 3 840 channels for each 1.875 GHz baseband.

The observations were carried out using 27 antennas in a compact configuration, implying we obtained baselines ranging from 15.8 m to 462.9 m (12.2 to 356.1 kλ). Standard calibration steps were applied to the data. The calibration sources associated to these observations were QSO J042315-012033 for band-pass calibration, and QSO J051002+180041 for gain and phase calibrations, and one antenna was flagged-out because of high system temperature. The observations consisted of 4 scans, which translates to a total time on source of 3.6 min for the field. After calibrating the set of raw visibilities, we applied one iteration of self-calibration in order to correct low-order phase calibration errors.

Deconvolving the set of visibilities with the CLEAN task implemented in CASA (McMullin et al. 2007) and using natural weighting we obtained the final images. The continuum image has an rms of 0.18 mJy/beam, with an elongated beam size of $0\farcs75 \times 1\farcs31$ and a position angle of $-48.6°$ (north-east). The mean rms associated to the individual ^{12}CO (2–1) channels is 21.1 mJy/beam per 0.635 km s^{-1} bin, after removing the continuum contribution in the visibility domain.

The continuum image shows a clear detection centered on the location of the faint companion, while it shows no significant emission from the binary system, confirming the

detection reported in K2015. The total flux from the third object is 3.4 ± 0.2 mJy. This detection is above the 1.78 ± 0.03 mJy reported by K2015 and in marginal agreement with the 4.5 ± 1.1 mJy at 850 μm measurement of Andrews & Williams (2005).

Similar to the continuum observations, we detected weak emission from ^{12}CO (2–1) gas located at the same position as the third object, with a SNR ~ 4 in three consecutive channels. This emission appears as a single peak line centered at 5.7 km s^{-1}, with a measured FWHM of 1.9 km s^{-1}, and a maximum of 72.8 mJy, based on a Gaussian fit to the line profile. The emission peaks from both the continuum and the integrated spectral line appear separated by 0.38 ± 0.16 arcsec (Fig. 1). Integrating our line profile over the corresponding channels we obtain a total flux of 156 mJy km s^{-1}.

3. Spectral Energy Distributions

The detection of gas around the third object in FW Tau is consistent with the proposed accreting nature of the disk and provides additional information to potentially constrain the properties of the third object. Before investigating this, we here summarize the observational data available for the triple system FW Tau with special emphasis on separating resolved and unresolved observations.

The SED of the full FW Tau system is dominated by emission from the photospheres of the central binary at wavelengths shorter than $\sim$15 μm. However, high resolution observations have also been able to identify the contribution from the third object in the J, H, K, and L bands (Kraus et al. 2014). Emission at 1.3 mm is also confirmed as originating from the third component, both in this paper and in previous observations (K2015). This study also find a lack of 1.3 mm flux from the central binary, allowing upper-limits to be derived for this component.

The excess emission at wavelengths longer than 15 μm and shorter than 1.3 mm is unresolved, i.e. it could stem from a circumbinary disk around the central binary and/or a disk around the third object. These unresolved observations cover the *Spitzer* photometry from Cieza et al. (2012), the *Herschel* data from Howard et al. (2013), and the 450 μm upper limit and 850 μm detection from Andrews & Williams (2005). Given the 1.3 mm detections of the third object, it is very likely that the later detection is also associated with it. Table 1 summarizes the photometric data available for the triple system FW Tau separating their different contributions.

4. Disk models

The first attempts to understand the nature of the third object in FW Tau object rapidly led to the hypothesis of it being a PMC (Kraus et al. 2014). However, as discussed in detail in K2015 it might also be a late-type stellar or sub-stellar companion embedded in an edge-on disk. We here confront both scenarios with the complete set of available observations by presenting an example model for each case. A complete parameter study is beyond the scope of this letter and not warranted given the limited quality of the current data.

For the SED analysis we assumed an extinction towards the line of sight of $A_V = 0.4$ (Kraus et al. 2014). We applied this correction to both the binary and third object photometry. The binary contribution was assumed to be the sum of two identical M5 dwarfs normalized to the J-band flux, with temperatures of $T_{\rm eff} = 3200\,{\rm K}$, masses of $M = 0.22\,M_\odot$ and a distance of 140 pc. These assumptions imply both stars have a radius of $1.1\,R_\odot$, suggesting an age of $\sim 2\,{\rm Myr}$ (Baraffe et al. 2015), which is in agreement with the Taurus age.

4.1. An edge-on disk around a substellar object

Assuming all the excess emission comes from the third object, the SED resembles that of an edge on disk around a (sub)stellar body. To model this possibility, we removed from the observed excesses the contributions from the central binary emission. Using the radiative transfer code MCFOST (Pinte et al. 2006, 2009) we find that for inclinations $i \gtrsim 85\,{\rm deg}$ the extinction on the central object is too high to agree with a spectral type later than M5 as required from spectroscopy (Bowler et al. 2014). Therefore, we focus on models with inclinations in the range of 70–85 deg, in which the disk has a direct effect on the central object emission as seen from our line of sight without causing too much extinction.

We explore various parameters for reproducing the SED, i.e. the disk dust mass $M_{\rm d}$, the scale height at 100 au H_0, flaring angle β, grain size distribution ($a_{\rm min}$, $a_{\rm max}$) for silicate composition, and the surface density exponent γ for a power-law disk geometry. We also explore different values for the temperature and luminosity of the central object. We fixed the size of the disk to be 100 au in diameter, in agreement with the maximum allowed by the non-resolved ALMA detections. The continuum emission is only weakly dependent on this assumption as the dust is optically thick only to a few tens of au, thus a smaller disk will still remain as a plausible alternative with small effects on the model SED. However, the gas emission is optically thick throughout, and will be affected by the assumed disk size. For all high inclination configurations we identify a degeneracy between the scale height,

flaring exponent, inclination, and central object mass, which makes the modeling of this disk particularly challenging. Nonetheless, we find that for most parameter combinations a dust mass of $\sim 3\,M_\oplus$ and a disk inner radius of ~ 1 au are required. Similarly, we find that an inclination close to $i \simeq 80.5$ deg is required, as slightly lower inclinations expose too much stellar flux and a slightly higher values extinct too much, making the model inconsistent with the observed SED. Although the mass of the central object is less constrained by the SED, it is possible to find reasonable representations of the SED for masses $\lesssim 0.14\,M_\odot$.

However, we can constrain the mass of the central object in the edge-on model if we require its age to be close to the one estimated for the central binary. The larger the assumed mass for the central object, the older it must be to reach agreement with the observations. Figure 2 shows this dependence, assuming the evolutionary models of Baraffe et al. (2015) and the calculated photospheric luminosity of $9 \times 10^{-3}\,L_\odot$. Even a conservative upper-limit of 6 Myr (~ 3 times the estimated age of the central binary) would imply the mass of the third object to be $\lesssim 60\,M_{\rm Jup}$. We can therefore rule out stellar masses but the third object might be a forming brown dwarf seen edge-on.

The detected ^{12}CO (2–1) emission might provide a further observational constraint on the nature of the third body. Therefore, we created an MCFOST radiative transfer model for the detected gas emission, assuming an ISM CO/H_2 abundance, a freezing temperature of 20 K (Qi et al. 2004; de Gregorio-Monsalvo et al. 2013), turbulent velocities ranging from 0.1–0.2 km s^{-1}, and the same spectral resolution as provided by the observations. We found that, given the low signal to noise of the line and the effects of photodissociation by the third object and the central binary (Williams & Best 2014), the total gas content of the disk remains an observationally unconstrained parameter.

Moreover, the shape of the line does not provide unambiguous observational constraints on the mass of the central object. For the spectral resolution given by our observations, masses $\gtrsim 35\,M_{\rm Jup}$ predict double-peaked lines in disagreement with the observed single-peaked line. However, we can not exclude such masses as the high noise level of the detection could have smeared out the line splitting. In addition, the observed line emission could be significantly affected by cloud contamination. Indeed, given that the measured velocity of the third object in FW Tau is close to the mean velocity of the Taurus cloud, i.e. ~ 7 km s^{-1} (Goldsmith et al. 2008), it is possible that either the blueshifted or redshifted emission from the disk and the cloud appear fused in the interferometer, thus precluding the interferometer from resolving the individual contributions and filtering them out (see e.g. Canovas et al. 2015). The same effect could explain the small (2.4σ) difference in position of the centers of the continuum and line detections (see §2).

As an example for an edge-on model that explains all the available observations, we

show a model fit to the SED and the CO line assuming a 5 Myr old 40 M_{Jup} third object in Fig. 3, where it is clear that all the observed excess flux can be explained by material confined to the third object.

4.2. A disk around a planetary mass companion object

The third object in FW Tau could also be a cooler low-mass object with a disk seen at low inclination. Indeed, the optical and near-IR emission is well fitted by a $T_{eff} \sim 1800$ K substellar model, with a luminosity implying a 1–2 Myr old age, in agreement with the age of Taurus forming objects, and consistent with a 5–7 M_{Jup} mass body (Baraffe et al. 2015).

The projected separation of the third object from the binary has been measured to be 330 au, and if the true separation is close to the projected one, the flux from the nearby binary will contribute to disk heating, thus affecting the temperature structure and consequently its emission. To reproduce the observed SED we have modeled the disk around the third component assuming the binary contribution to be identical to that described in §4.1. The separation between the binary stars was assumed to be 11 au, whereas the distance and the relative orientation of the binary with respect to the disk were changed in order to explore different configurations for the external illumination. Apart from this additional parameter we explored the same parameter space as in §4.1.

We find that the SED of FW Tau can be explained with models in which the binary illuminates the disk with an incident angle $\sim 20 - 50$ deg with respect to the disk plane as these orientations maximize the heating of the disk (Fig. 3). Other configurations do not expose the disk to enough radiation, creating a lack of emission at longer wavelengths. We find that $\sim 2 - 3\,M_{\oplus}$ of dust are enough to reproduce the emission at (sub) mm-wavelengths, in agreement with the estimates of K2015. The mid/far-IR emission is consistent with very small flaring angle exponents (i.e. $\beta \simeq 1.0$), and an inner radius of ~ 0.3 au. The overall flux excess is only achieved, however, by introducing a relatively large scale height ($\sim 22 - 25$ au at 100 au), and models with smaller values tend to underestimate the mid/far-IR emission.

Concerning the gas line, for an assumed central body mass of 7 M_{Jup}, the spectral profile appears as a clear single line for inclinations $i \lesssim 15$ deg, in agreement with the observations (see Fig. 3), and the Keplerian double-peak appears only for larger inclinations. The amplitude of the CO line peak suggests a very small gas mass, because the amplitude of the line predicted by the model, for an ISM CO/H_2 abundance and gas-to-dust mass ratio, is much larger than the observed values. This could be either an effect of CO photodissociation which can reduce the CO/H_2 abundance (Visser et al. 2009; Williams & Best 2014), an

intrinsic very low gas-to-dust mass ratio, and/or a smaller disk size because a smaller emitting area would predict less CO flux and thus require a less reduced gas content. Similar to the high-inclination case, it is also possible that the lack of flux from the observations compared to the model might be due to the interferometer filtering out a major fraction of the flux.

5. Conclusion

We present ALMA Cycle 1 band 6 continuum and ^{12}CO (2–1) observations of the triple system FW Tau and test two different scenarios against the new observations.

We find that the edge-on model can recreate all observed excess emission. Although the observed single-peaked line is most naturally reproduced assuming a low mass for the third object, larger masses can not be excluded because of the low SNR of the detection and the possibility of cloud contamination. Assuming the third object and its central binary are coeval however, evolutionary tracks strongly suggest it is a substellar object.

The low inclination scenario for a planetary mass object, in combination with the radiation received from the close binary, is capable of reproducing the SED and the single-peaked line emission. The weakness of the ^{12}CO (2–1) line either indicates a low gas mass, significant photodissociation affecting the CO/H_2 abundance, significant contamination by the cloud, a smaller disk, or a combination of these four effects are at work.

Resolved continuum observations of both the binary and third components of the FW Tau system, as well as resolved optically thin line detections including both CO higher-transition and isotopologues, will definitively unveil the nature of this intriguing system. Regardless, all data suggest FW Tau is a substellar object caught in formation, cementing its position as a vital object for understanding the brown dwarf/planet formation process.

C.C. and M.R.S. acknowledge the support from CONICYT FONDECYT grants 3140592 and 1141269 respectively. C.C., and H.C. acknowledge support from ALMA-CONICYT grant 31130027. C.C., A.H., M.R.S., H.C., L.C. acknowledge support from the Millennium Nucleus RC130007 (Chilean Ministry of Economy). This paper makes use of the following ALMA data: ADS/JAO.ALMA#2012.1.00350.S. ALMA is a partnership of ESO (representing its member states), NSF (USA) and NINS (Japan), together with NRC (Canada), NSC and ASIAA (Taiwan), and KASI (Republic of Korea), in cooperation with the Republic of Chile. The Joint ALMA Observatory is operated by ESO, AUI/NRAO and NAOJ. The National Radio Astronomy Observatory is a facility of the National Science Foundation operated under cooperative agreement by Associated Universities Inc. This publication makes

use of data products from the Wide-field Infrared Survey Explorer, which is a joint project of the University of California, Los Angeles, and the Jet Propulsion Laboratory/California Institute of Technology, funded by the National Aeronautics and Space Administration.

REFERENCES

Andrews, S. M., & Williams, J. P. 2005, ApJ, 631, 1134

Bailey, V., Meshkat, T., Reiter, M., et al. 2014, ApJ, 780, L4

Baraffe, I., Chabrier, G., Allard, F., & Hauschildt, P. H. 2002, A&A, 382, 563

Baraffe, I., Homeier, D., Allard, F., & Chabrier, G. 2015, A&A, 577, A42

Boss, A. P. 1997, Science, 276, 1836

—. 2011, ApJ, 731, 74

Bowler, B. P., Liu, M. C., Kraus, A. L., & Mann, A. W. 2014, ApJ, 784, 65

Canovas, H., Schreiber, M. R., Cáceres, C., et al. 2015, ArXiv e-prints, arXiv:1503.04821

Chabrier, G., Baraffe, I., Allard, F., & Hauschildt, P. 2000, ApJ, 542, 464

Cieza, L. A., Schreiber, M. R., Romero, G. A., et al. 2012, ApJ, 750, 157

Cieza, L. A., Padgett, D. L., Allen, L. E., et al. 2009, ApJ, 696, L84

de Gregorio-Monsalvo, I., Ménard, F., Dent, W., et al. 2013, A&A, 557, A133

Goldsmith, P. F., Heyer, M., Narayanan, G., et al. 2008, ApJ, 680, 428

Howard, C. D., Sandell, G., Vacca, W. D., et al. 2013, ApJ, 776, 21

Ireland, M. J., Kraus, A., Martinache, F., Law, N., & Hillenbrand, L. A. 2011, ApJ, 726, 113

Kratter, K. M., Murray-Clay, R. A., & Youdin, A. N. 2010, ApJ, 710, 1375

Kraus, A. L., Andrews, S. M., Bowler, B. P., et al. 2015, ApJ, 798, L23

Kraus, A. L., Ireland, M. J., Cieza, L. A., et al. 2014, ApJ, 781, 20

Lafrenière, D., Jayawardhana, R., & van Kerkwijk, M. H. 2008, ApJ, 689, L153

Lissauer, J. J., & Stevenson, D. J. 2007, Protostars and Planets V, 591

McMullin, J. P., Waters, B., Schiebel, D., Young, W., & Golap, K. 2007, in Astronomical Society of the Pacific Conference Series, Vol. 376, Astronomical Data Analysis Software and Systems XVI, ed. R. A. Shaw, F. Hill, & D. J. Bell, 127

Neuhäuser, R., Guenther, E. W., Wuchterl, G., et al. 2005, A&A, 435, L13

Pinte, C., Harries, T. J., Min, M., et al. 2009, A&A, 498, 967

Pinte, C., Ménard, F., Duchêne, G., & Bastien, P. 2006, A&A, 459, 797

Qi, C., Ho, P. T. P., Wilner, D. J., et al. 2004, ApJ, 616, L11

Schmidt, T. O. B., Neuhäuser, R., Seifahrt, A., et al. 2008, A&A, 491, 311

Seifahrt, A., Neuhäuser, R., & Hauschildt, P. H. 2007, A&A, 463, 309

Siess, L., Dufour, E., & Forestini, M. 2000, A&A, 358, 593

Visser, R., van Dishoeck, E. F., & Black, J. H. 2009, A&A, 503, 323

White, R. J., & Ghez, A. M. 2001, ApJ, 556, 265

Williams, J. P., & Best, W. M. J. 2014, ApJ, 788, 59

Wright, E. L., Eisenhardt, P. R. M., Mainzer, A. K., et al. 2010, AJ, 140, 1868

Zhou, Y., Herczeg, G. J., Kraus, A. L., Metchev, S., & Cruz, K. L. 2014, ApJ, 783, L17

Table 1. FW Tau photometry data

Wavelength (μm)	Flux FW Tau A/B	Flux Third component	Flux Unresolved	Unit	Reference[a]
1.25	10.34	17.34 ± 0.07	···	mag	1
1.66	9.67	16.24 ± 0.07	···	mag	1
2.20	9.38	15.29 ± 0.07	···	mag	1
3.35	···	···	9.196 ± 0.026	mag	2
3.6	···	···	64.8 ± 0.3	mJy	3
3.8	9.19	14.25 ± 0.10	···	mag	1
4.5	···	···	44.8 ± 0.1	mJy	3
4.6	···	···	41.5 ± 1.0	mJy	2
5.8	···	···	32.4 ± 0.2	mJy	3
8.0	···	···	18.0 ± 0.1	mJy	3
12	···	···	8.2 ± 0.3	mJy	2
22	···	···	< 10.5	mJy	2
24	···	···	6.79 ± 0.4	mJy	4
70	···	···	30 ± 4	mJy	5
100	···	···	33 ± 4	mJy	5
160	···	···	70 ± 40	mJy	5
450	···	···	< 30.0	mJy	6
850	···	···	4.5 ± 1.1	mJy	6
1300	< 0.084	1.78 ± 0.03	···	mJy	7
1300	···	3.4 ± 0.2	···	mJy	This work

Note. — [a]References: (1) Kraus et al. (2014); (2) Wright et al. (2010); (3) Cieza et al. (2009); (4) Cieza et al. (2012); (5) Howard et al. (2013); (6) Andrews & Williams (2005); (7) Kraus et al. (2015).

Table 2. Parameters in the models

Parameter	PMC model	Edge-on disk model	Unit
i	10	80.5	deg
$M_{\rm S}$	7	40	$M_{\rm Jup}$
$M_{\rm disk}$	3	3	$M_{\oplus}$
H_0	25	15	au
β	1.00	1.25	···
γ	-0.65	-0.1	···
$a_{\rm min}$	1.0×10^{-2}	1.0×10^{-2}	μm
$a_{\rm max}$	1.0×10^{3}	1.0×10^{3}	μm

Note. — These are the parameters used to create the models shown in Fig. 3.

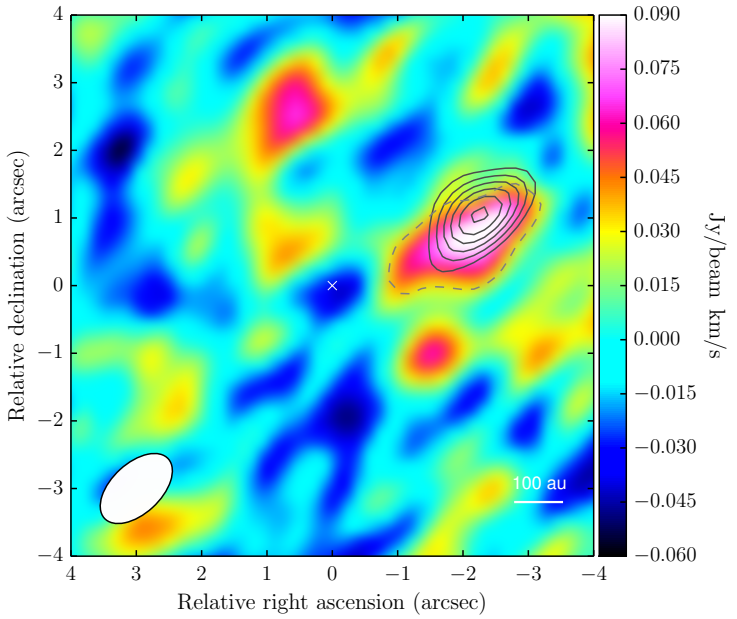

Fig. 1.— Integrated ^{12}CO(2-1) emission map. The solid-line contours show the continuum detection above 5σ in steps of 2σ. The dashed contour limits the 3σ emission from the ^{12}CO (2–1) line used to calculate the line profile. The white ellipse shows the synthesized ALMA beam.

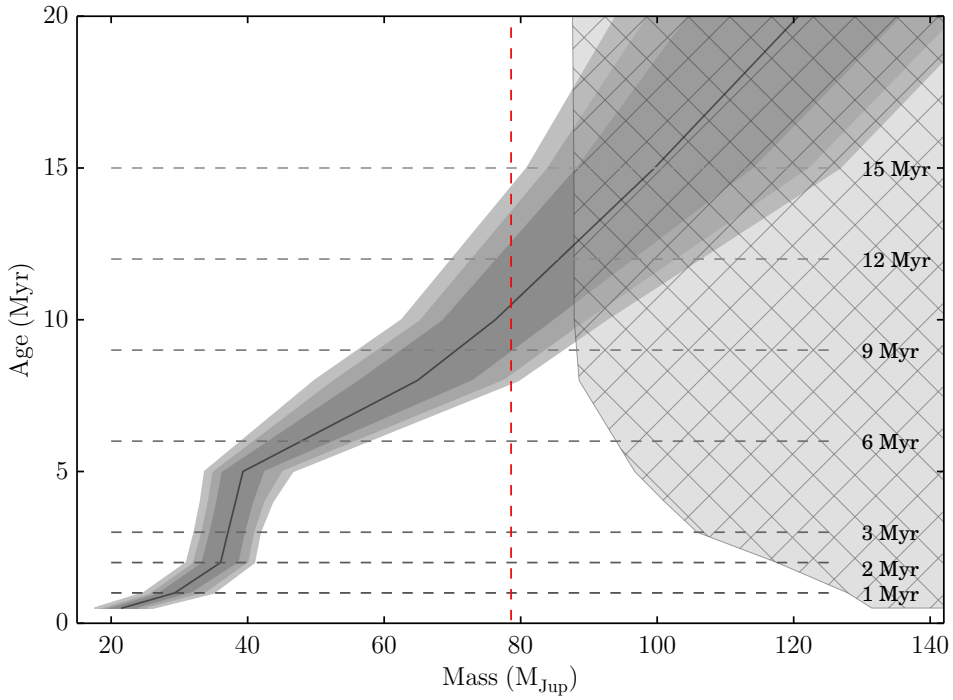

Fig. 2.— Age-mass region constrained by the edge-on modeling. Gray regions represent the $1-3\sigma$ range of allowed ages for a given central object mass. The red-dashed line indicates the deuterium-burning limit mass for a solar composition (Chabrier et al. 2000). The shaded area limits the maximum allowed mass given spectroscopic constraints (Bowler et al. 2014).

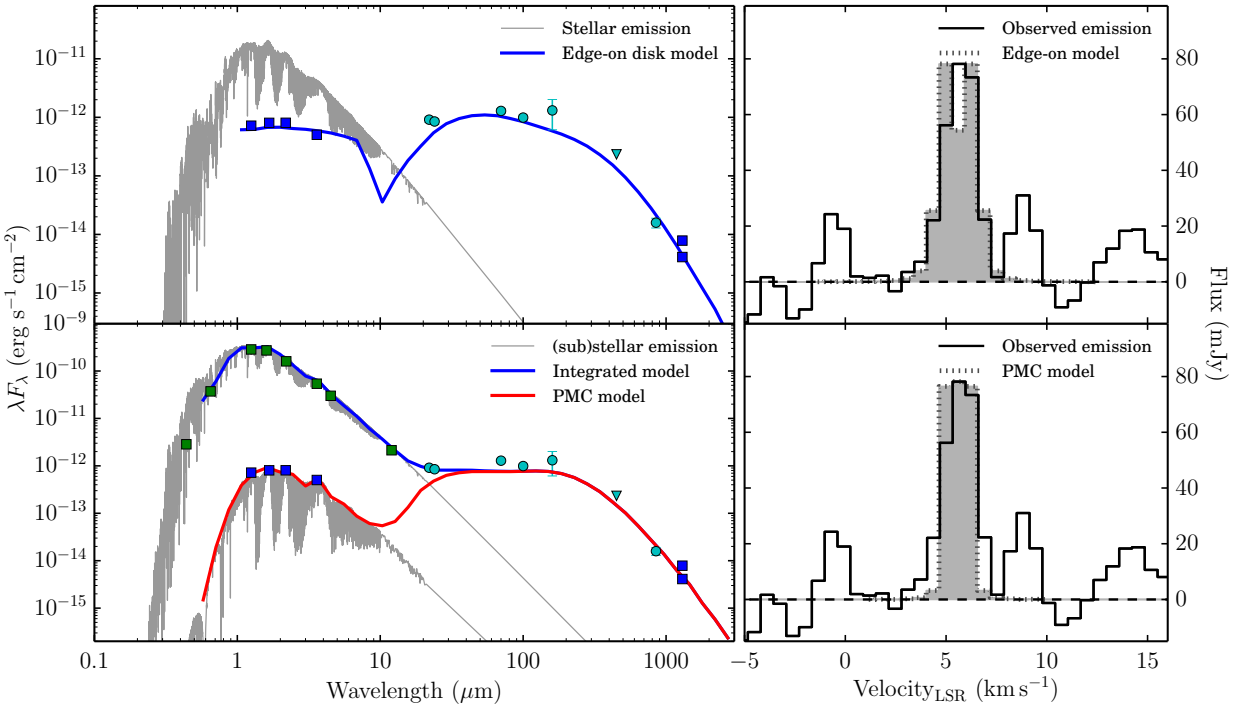

Fig. 3.— *Left panels*: SED for the FW Tau system. Green squares represent the emission from the central binary, blue squares represent the emission associated to the third component, cyan circles and triangle are the unresolved photometric observations and upper limit respectively. Upper-left panel shows the edge-on model described in §4.1 (blue solid line), including the highly absorbed substellar photosphere (gray solid line). Lower-left panel shows the PMC model (red solid line) including the photospheric emission from a 1800 K central object, and the integrated SED model composed of the PMC model plus the photospheric emission from the central binary, shown as M5-type photospheres (§4.2). The parameters used to create these models are specified in Table 2. *Right panels*: Detected ALMA ^{12}CO (2–1) line profile measured over the 3σ region shown in Fig. 1 (black solid line). The dotted lines represent the edge-on model (§4.1; upper-right panel), and the planetary mass companion model (§4.2; lower-right panel), respectively. The unconstrained total gas mass was adjusted to fit the maximum detected emission.